Adaptive Control for Pneumatic Artificial Muscle Systems With Parametric Uncertainties and Unidirectional Input Constraints

Ning Sun, *Member, IEEE*, Dingkun Liang, Yiming Wu, Yiheng Chen, Yanding Qin, and Yongchun Fang, *Senior Member, IEEE*

***Abstract*—Pneumatic artificial muscle (PAM) systems are a kind of tube-like actuators, which can act roughly like human muscles by performing contractile or extensional motions actuated by pressurized air. At present, it is still an open and challenging issue to tackle positioning and tracking control problems of PAM systems, due to inherent characteristics, e.g., unidirectional inputs, high nonlinearities, hysteresis, time-varying characteristics, etc. In this paper, a new adaptive control method is proposed for PAM systems, which achieves satisfactory tracking performance. To this end, an update law is designed to estimate unknown system parameters online. Also, some control input transforming operations are applied to address unidirectional constraints (i.e., control inputs of PAM systems should always be positive). As far as we know, compared with most of the existing control methods, this paper gives the *first continuous* control solution for PAM systems that can *simultaneously* compensate parametric uncertainties, reject external disturbances, and meet unidirectional constraints. *Without* linearizing the nonlinear dynamics, the closed-loop system is theoretically proven to be asymptotically stable at the equilibrium point with the stability analysis. In addition, a series of hardware experiments are implemented on a self-built hardware platform, indicating that the proposed method achieves satisfactory tracking control and exhibits robustness against parametric uncertainties and disturbances.**

***Index Terms*—Lyapunov techniques, mechatronics, pneumatic artificial muscle (PAM) systems, unidirectional input constraint.**

Manuscript received March 28, 2019; accepted May 23, 2019. Date of publication June 19, 2019; date of current version January 14, 2020. This work was supported in part by the National Key R&D Program of China under Grant 2018YFB1309000, in part by the National Natural Science Foundation of China under Grant 61873134 and Grant U1706228, in part by the Young Elite Scientists Sponsorship Program by Tianjin under Grant TJSQNTJ-2017-02, and in part by the Japan Society for the Promotion of Science International Research Fellow Program under Grant 18F18363. Paper no. TII-19-1086. *(Corresponding author: Yongchun Fang.)*

The authors are with the Institute of Robotics and Automatic Information Systems, College of Artificial Intelligence, and the Tianjin Key Laboratory of Intelligent Robotics, Nankai University, Tianjin 300350, China (e-mail: sunn@nankai.edu.cn; liangdk@mail.nankai.edu.cn; ymwu@mail.nankai.edu.cn; chenyh@mail.nankai.edu.cn; qinyd@nankai.edu.cn; fangyc@nankai.edu.cn).

Color versions of one or more of the figures in this paper are available online at http://ieeexplore.ieee.org.

Digital Object Identifier 10.1109/TII.2019.2923715

I. Introduction

In THE field of modern industry, various mechatronic systems with nonlinear characteristics [1]–[6] are widely used. Pneumatic artificial muscle (PAM) systems are a special kind of nonlinear systems, which can contract or extend like real human muscles by inflating and deflating pressurized air through servo valves [7]. The special working principle of PAM systems brings many advantages for applications, e.g., flexible tubular structures, lightweight materials, high power-to-weight/volume ratios, clean power, etc. [7]–[12]. Based on these merits, PAM systems are mainly applied to micromanipulation robots and biomimetic rehabilitation robots. However, the force generated by pressurized air inside PAM systems also brings complicated inherent characteristics, such as high nonlinearities, complex hysteresis, and time-varying characteristics, which make the control issues challenging and nontrivial.

At present, there mainly exist two types of models to depict PAM systems' dynamic characteristics: the theoretical model [13]–[16] and the phenomenological model [17]–[21]. The theoretical model is strongly related to geometric structures and material properties of PAM systems, which can be obtained by using some methods of mathematical physics (e.g., the virtual work principle, the force-balance principle, etc.). Hence, the theoretical model is complicated and contains a number of system parameters [13]–[16]. In contrast, the phenomenological model of PAM systems mainly analyzes the relationship between system inputs and outputs; commonly, the phenomenological model consists of two kinds of models: the Colbrunn model [17] and the Reynolds model [18]. In particular, the Reynolds model is the most commonly used phenomenological model, which is established by the Voigt viscoelastic model, and considers that a PAM system consists of three parallel elements, i.e., a spring element, a damping element, and a contractile element [18]–[21].

Based on both theoretical and phenomenological models of PAM systems, in order to achieve the control objective of positioning tracking, some feedback control strategies are proposed in the literature [21]–[23]. Specifically, Merola *et al.* combine a proportional-integral-derivative (PID) control scheme for PAM systems with a feedforward term to track reference trajectories [21]. Furthermore, Minh *et al.* propose a feedforward path of a cascade position control scheme for PAM systems with

1551-3203 © 2019 IEEE. Personal use is permitted, but republication/redistribution requires IEEE permission.
See http://www.ieee.org/publications_standards/publications/rights/index.html for more information.

Authorized licensed use limited to: Kent State University Libraries. Downloaded on September 20,2023 at 17:54:05 UTC from IEEE Xplore. Restrictions apply.

hysteresis compensation [23]. Additionally, in practical applications, PAM systems usually suffer from external disturbances and uncertainties (e.g., unknown parameters, unmodeled uncertainties, etc.), which may degrade the control performance during real-time tracking control. In order to deal with the uncertainties and improve the robustness of PAM systems, some control methods are developed, such as fuzzy logic controllers, adaptive methods, and sliding-mode strategies [24]–[29]. More specifically, Chen and Shih design a visual fuzzy control method for automatic manipulation systems with PAM systems under the microscope vision [24]. Zhang *et al.* develop an active model-based control scheme to identify the system parameters and achieve position tracking control by using a nonlinear PID scheme [25]. In addition, an integrated intelligent nonlinear control scheme is proposed for PAM systems, combined with sliding-mode and backstepping techniques [26].

Nevertheless, the study of PAM systems is still at an early stage, and there still exist many nontrivial and open control issues to be addressed.

1) Practically, in the presence of nonlinear time-varying characteristics, it is usually difficult to obtain accurate real-time model parameters of PAM systems, especially when the air pressure changes during the entire control process.
2) Also, PAM systems usually suffer from uncertainties and external disturbances, which degrade the control performance.
3) Furthermore, when the pressurized air enters inner rubber tubes of PAM systems, the "muscle" contracts along the longitudinal direction; in other words, the pressurized air only provides contractile forces through the inflation process, and the "muscle" tends to extend to its original states naturally during the deflation process. It means that the control input (corresponding to the pressurized air) of PAM systems is constrained to be *nonnegative*. However, there is no reported control-related works of PAM systems, which consider unidirectional input constraints in this paper.

To handle the abovementioned important issues, in this paper, an adaptive control method is proposed for PAM systems, which achieves satisfactory tracking performance and can effectively deal with the influence induced by parametric uncertainties and external disturbances. First, unidirectional constraints are considered and "removed." Then, an adaptive update law is designed to compensate unknown parameters by online estimation. Furthermore, a *continuous* robust controller is proposed on the basis of the estimated system parameters to track various reference trajectories. Compared with traditional sliding-mode controllers, the chattering problem is avoided by elaborately designing a continuous control input. In addition, the stability analysis is provided in detail. The main contributions of this paper can be summarized as follows.

1) The proposed adaptive controller can achieve fast and accurate positioning with satisfactory tracking performance for PAM systems, which can *simultaneously* take into consideration several practical problems, such as parametric uncertainties, external disturbances, physical constraints, etc. It indicates that the proposed method guarantees satisfactory robustness and can adapt to some different unfavorable working conditions.
2) By elaborated design, the dual requirements of continuity (in control inputs) and robustness are respected, and the proposed controller has a continuous expression, which is smoother than traditional sliding-mode control, and consequently, the generated control commands are easier to execute. Moreover, for both controller design and stability analysis, *no* linearization operations to the nonlinear dynamics are needed, which is theoretically important.
3) The Lyapunov-based stability analysis is implemented to theoretically support the proposed controller, and moreover, a series of hardware experiments are carried out to practically validate its satisfactory performance.

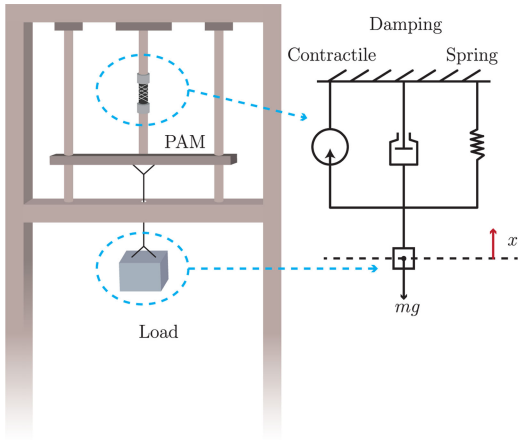

Fig. 1. Model of PAM systems.

The rest of this paper is organized as follows. First, in Section II, based on the three-element model of PAM systems, some transforming operations are given. Second, the entire control method design process is provided in detail in Section III. Furthermore, in Section IV, the Lyapunov-based stability analysis is provided. Furthermore, hardware experiments are implemented on a self-built hardware platform in Section V. Finally Section VI concludes this paper.

II. Problem Formulation

The model of PAM systems is shown in Fig. 1, and precisely, Fig. 2 shows the contractile/extensional motions of the "muscle" when inflating/deflating pressurized air. The control objective is to actuate PAM systems to track various reference trajectories, so as to further complete actuating tasks, in the presence of complicated inherent PAM systems' dynamic characteristics, external disturbances, and parametric uncertainties. First, the three-element model of PAM systems is given as follows [25]:

$$m\ddot{x} + (d_1 p_m + d_0)\,\dot{x} + (s_{11} p_m + s_{10})\,x + (s_{21} p_m + s_{20})\,x^2 = f_{c1} p_m + f_{c0} - mg \tag{1}$$

where $m, g, p_m(t)$, and $x(t)$ denote the load mass, the gravitational acceleration, the air pressure, and the length variation (corresponds to the load displacement), respectively, d_1 and d_0

Authorized licensed use limited to: Kent State University Libraries. Downloaded on September 20,2023 at 17:54:05 UTC from IEEE Xplore. Restrictions apply.

Fig. 2. Contractile and extensional motions of PAM systems.

are damping coefficients, $s_{11}, s_{10}, s_{21},$ and s_{20} are second-order spring model-related coefficients, and f_{c1} and f_{c0} are muscle contractile force coefficients. Precisely, the air pressure inside PAM systems can be expressed as

$$p_m = p_0 + p \tag{2}$$

where p_0 is the nominal atmospheric pressure and $p(t)$ is the pressure of the injected air. Actually, the values of m and f_{c1} in (1) *cannot* be obtained precisely, which can be expressed as follows:

$$m = m_0 + \Delta m, \quad f_{c1} = f_{ce} + \Delta f_{c1} \tag{3}$$

where m_0 and Δm are the nominal mass and the uncertain part of m, respectively, and f_{ce} and Δf_{c1} represent the nominal value and the mismatch of f_{c1}, respectively. By inserting (2) and (3) into (1), the model listed in (1) can be transformed into a new form as follows:

$$\begin{aligned}(m_0 + \Delta m)\,\ddot{x} = &-\left(d_1\dot{x} + s_{11}x + s_{21}x^2\right)p + f_{c1}p_0 + f_{c0} \\ &- (d_1p_0 + d_0)\,\dot{x} - (s_{11}p_0 + s_{10})\,x \\ &- (s_{21}p_0 + s_{20})\,x^2 - (m_0 + \Delta m)\,g \\ &+ (f_{ce} + \Delta f_{c1})\,p. \end{aligned} \tag{4}$$

Then, dividing both sides of (4) by $m_0 + \Delta m$, one has

$$\begin{aligned}\ddot{x} = &\frac{f_{c1}p_0 + f_{c0}}{m_0 + \Delta m} - g - \frac{d_1p\dot{x} + s_{11}px + s_{21}px^2}{m_0 + \Delta m} \\ &- \frac{(d_1p_0 + d_0)\,\dot{x} + (s_{11}p_0 + s_{10})\,x + (s_{21}p_0 + s_{20})\,x^2}{m_0 + \Delta m} \\ &+ \frac{f_{ce} + \Delta f_{c1}}{m_0 + \Delta m}p \\ = &-\frac{(d_1p_0 + d_0)\,\dot{x} + (s_{11}p_0 + s_{10})\,x + (s_{21}p_0 + s_{20})\,x^2}{m_0 + \Delta m} \\ &+ \frac{f_{c1}p_0 + f_{c0}}{m_0 + \Delta m} + \frac{f_{ce}}{m_0}p - \left(\frac{f_{ce}}{m_0}p - \frac{f_{c1}}{m_0 + \Delta m}p\right) \\ &- g - \frac{d_1p\dot{x} + s_{11}px + s_{21}px^2}{m_0 + \Delta m}. \end{aligned} \tag{5}$$

Since PAM systems are powered by the pressure of the air, the air pressure $p(t)$ is regarded as the input, which can *only* work during the inflation process; in other words, the unidirectional constraint of $p(t)$ must be respected. As we know, due to physical constraints, if the control input $p(t)$ exceeds the applicable ranges, PAM systems will fall into saturation, and the control performance will be degraded. To this end, $p(t)$ can be expressed as follows:

$$p \triangleq F(u) = \begin{cases} 0, & u \le 0 \\ u, & 0 \le u < u_{\max} \\ u_{\max}, & u \ge u_{\max} \end{cases} \tag{6}$$

where $u(t)$ is the control input to be designed, $u_{\max}$ is the maximum value of $u(t)$, and $p = F(u)$ is the (ultimate) real control input working on the system. As shown in (6), we can find that, regardless of the specific expressions of $u(t)$, the air pressure $p(t)$ will always be *nonnegative*. To facilitate the subsequent controller design process, $F(u)$ is reexpressed as follows:

$$F(u) = u + \Delta u \tag{7}$$

where $\Delta u \triangleq F(u) - u$ is introduced to analyze the effects of unidirectional input constraints. Then, by inserting (7) into (5), the following equation can be derived:

$$\ddot{x} = -g + wu + \left(a_1\dot{x} + a_2x + a_3x^2\right) + \xi \tag{8}$$

where

$$\begin{aligned} a_1 &= -\frac{d_1p_0 + d_0}{m_0 + \Delta m}, \quad a_2 = -\frac{s_{11}p_0 + s_{10}}{m_0 + \Delta m} \\ a_3 &= -\frac{s_{21}p_0 + s_{20}}{m_0 + \Delta m} \\ \xi &= \frac{\left[f_{c1} - w\,(m_0 + \Delta m) - \left(d_1\dot{x} + s_{11}x + s_{21}x^2\right)\right]F(u)}{m_0 + \Delta m} \\ &\quad + \frac{w\,(m_0 + \Delta m)\,\Delta u + f_{c1}p_0 + f_{c0}}{m_0 + \Delta m} \\ w &= \frac{f_{ce}}{m_0}. \end{aligned} \tag{9}$$

To simplify the subsequent controller design, $\xi(t)$ can be considered as a lumped term of uncertain disturbances, which will be subsequently addressed by designing an elaborate control law for $u(t)$. It is not difficult to find that the mismatch term $\Delta u(t)$ is included in $\xi(t)$, which will also be analyzed by the proposed control method during the stability analysis. In (9), $a_1, a_2,$ and a_3 are uncertain model parameters to be estimated subsequently.

III. Controller Design

The dynamic model (8) can be transformed into the following form:

$$\begin{aligned}\ddot{x} &= -g + wu + \boldsymbol{q}\boldsymbol{\theta} + \xi \\ &= -g + wu + \boldsymbol{q}_d\boldsymbol{\theta} + \xi_1 \end{aligned} \tag{10}$$

Authorized licensed use limited to: Kent State University Libraries. Downloaded on September 20,2023 at 17:54:05 UTC from IEEE Xplore. Restrictions apply.

where

$$\xi_1 = \xi - \boldsymbol{q}_d\boldsymbol{\theta} + \boldsymbol{q}\boldsymbol{\theta}, \quad \boldsymbol{q} = [\dot{x}, x, x^2]$$
$$\boldsymbol{q}_d = [\dot{x}_d, x_d, x_d^2], \quad \boldsymbol{\theta} = [a_1, a_2, a_3]^{\mathrm{T}}. \tag{11}$$

In (11), $x_d(t)$ is the desired reference trajectory of $x(t)$; $\boldsymbol{q}_d$ is the desired regression matrix, which contains some known functions, e.g., $x_d(t)$ and $\dot{x}_d(t)$, which can be derived through offline calculations in advance to reduce online computations; $\xi_1(t)$ denotes the lumped disturbance term consisting of unknown disturbances, including uncertainties, external disturbances, etc.; as a result, modeling for external disturbances is not required. As for $x_d(t), \xi_1(t)$ and their derivatives, it is practically assumed that

$$x_d, \dot{x}_d, \ddot{x}_d, \dddot{x}_d, x_d^{(4)}, \quad \xi_1, \dot{\xi}_1, \ddot{\xi}_1 \in \mathcal{L}_\infty. \tag{12}$$

From (12), it is indicated that the reference trajectory $x_d(t)$, the lumped disturbance $x_d(t)$, and their derivatives are bounded, which are reasonable practical assumptions [30]–[32]. It is also noted that, since the Lyapunov-based control design and analysis are conservative by nature, the proposed control method may also work well in practice even if these assumptions are not rigorously satisfied. On the basis of the transformed model (10) with unknown system parameters in the presence of external disturbances, and motivated by [33] and [34], an adaptive robust controller will be developed for PAM systems to track trajectories and deal with uncertainties and disturbances. First, to deal with unknown parameters in (10), the control law $u(t)$ is divided into two parts, $u_1(t)$ and $u_2(t)$, such that

$$u = (u_1 + u_2)/w. \tag{13}$$

Specifically, $u_1(t)$ is given as

$$u_1 = -\boldsymbol{q}_d\hat{\boldsymbol{\theta}} \tag{14}$$

where $\hat{\boldsymbol{\theta}}(t) = [\hat{a}_1, \hat{a}_2, \hat{a}_3]^{\mathrm{T}}$ denotes the estimation of $\boldsymbol{\theta}(t)$ in (11). By inserting (13) and (14) into (10), and making some mathematical arrangements, it can be derived that

$$\ddot{x} = -g + u_2 + \boldsymbol{q}_d\tilde{\boldsymbol{\theta}} + \xi_1 \tag{15}$$

where $\tilde{\boldsymbol{\theta}} = \boldsymbol{\theta} - \hat{\boldsymbol{\theta}}$. By increasing the order of (15), the third-order time derivative of $x(t)$ can be obtained as follows:

$$\dddot{x} = \dot{u}_2 + \dot{\boldsymbol{q}}_d\tilde{\boldsymbol{\theta}} + \boldsymbol{q}_d\dot{\tilde{\boldsymbol{\theta}}} + \dot{\xi}_1. \tag{16}$$

Based on the augmented dynamic model in (16), the derivative of $u_2(t)$, i.e., $\dot{u}_2(t)$, is regarded as a virtual input to be further designed. The control objective is to make $x(t)$ track the desired trajectory $x_d(t)$, in the presence of unidirectional control inputs, parametric uncertainties, and disturbances.

First, the tracking error is defined as follows:

$$e \triangleq x - x_d. \tag{17}$$

By inserting (16) into (17) and making some arrangements, it can be obtained that

$$\dddot{e} = \dddot{x} - \dddot{x}_d = \dot{u}_2 + \dot{\boldsymbol{q}}_d\tilde{\boldsymbol{\theta}} + \boldsymbol{q}_d\dot{\tilde{\boldsymbol{\theta}}} + \dot{\xi}_1 - \dddot{x}_d. \tag{18}$$

To prevent the *unmeasurable* acceleration terms from being injected into $\dot{u}_2(t)$, and to facilitate the subsequent controller design and the theoretical analysis, we also define some auxiliary error signals as follows:

$$e_1 = \dot{e} + \lambda_1 e, \dot{e}_2 = -\lambda_2 e_2 + e_3$$
$$\dot{e}_3 = -e_3 - (k_0 + 1)r_2 + e_1 - e_2 \tag{19}$$

where $\lambda_1, \lambda_2,$ and k_0 are positive constants, and $r_2(t)$ is an auxiliary signal to be further defined. Then, based on (19), the following auxiliary signals are provided:

$$r_1 = e_1 + e_2, \quad r_2 = \dot{r}_1 + \lambda_2 r_1 = \dot{e}_1 + \lambda_2 e_1 + e_3. \tag{20}$$

Based on (20), the update law in (14) can be designed as follows:

$$\dot{\hat{\boldsymbol{\theta}}} = \boldsymbol{\beta}\dot{\boldsymbol{q}}_d^{\mathrm{T}} r_2 \tag{21}$$

where $\boldsymbol{\beta} \in \mathbb{R}^{3\times 3}$ is a positive-definite constant diagonal matrix. Furthermore, by taking the derivative of $r_2(t)$ in (20), and inserting (18) and (19), the signal $\dot{r}_2(t)$ can be derived as

$$\begin{aligned}\dot{r}_2 &= \dddot{e} + \lambda_1\ddot{e} + \lambda_2\dot{e}_1 + \dot{e}_3 \\ &= \left(\dot{u}_2 + \dot{\boldsymbol{q}}_d\tilde{\boldsymbol{\theta}} + \boldsymbol{q}_d\dot{\tilde{\boldsymbol{\theta}}} + \dot{\xi}_1 - \dddot{x}_d\right) + \lambda_1\ddot{e} + \lambda_2\dot{e}_1 - e_3 \\ &\quad - (k_0 + 1)r_2 + e_1 - e_2 + (e_1 - e_1 + r_2 - r_2) \\ &= \left(\dot{\xi}_1 - \dddot{x}_d + \lambda_1\ddot{e} + \lambda_2\dot{e}_1 - e_3 + e_1 - e_2 - \boldsymbol{q}_d\dot{\hat{\boldsymbol{\theta}}}\right) \\ &\quad + (e_1 + r_2) - (k_0 + 1)r_2 - e_1 - r_2 + \dot{\boldsymbol{q}}_d\tilde{\boldsymbol{\theta}} + \dot{u}_2\end{aligned} \tag{22}$$

where the term $e_1 - e_1 + r_2 - r_2$ introduced in (22) will further be separated into two parts (i.e., $e_1 + r_2$ and $-e_1 - r_2$), which can cancel the cross terms in the subsequent Lyapunov-based stability analysis. To facilitate the stability analysis, we define

$$\begin{aligned}H\left(x, \dot{x}, \ddot{x}, e_2, e_3, r_2, t\right) &\triangleq \dot{\xi}_1 - \dddot{x}_d + \lambda_1\ddot{e} + \lambda_2\dot{e}_1 - e_3 + e_1 \\ &\quad - e_2 - \boldsymbol{q}_d\dot{\hat{\boldsymbol{\theta}}} + e_1 + r_2.\end{aligned} \tag{23}$$

After applying the update law (21) and making some arrangements, $H(t)$ can be divided into two auxiliary functions $H_d(t)$ and $H_1(t)$, such that

$$\begin{aligned}H_d &= H\left(x_d, \dot{x}_d, \ddot{x}_d, 0, 0, 0, t\right) \\ H_1 &= H - H_d = \left(\dot{\xi}_1 - \dot{\xi}_{1d}\right) + \lambda_1\ddot{e} + \lambda_2\dot{e}_1 - e_3 \\ &\quad + 2e_1 - e_2 + r_2 - \boldsymbol{q}_d\boldsymbol{\beta}\dot{\boldsymbol{q}}_d^{\mathrm{T}} r_2\end{aligned} \tag{24}$$

where $\dot{\xi}_{1d} = \dot{\xi}_1\left(x_d, \dot{x}_d, \ddot{x}_d, 0, 0, 0, t\right)$. Then, (22) can be transformed into a simpler form as follows:

$$\dot{r}_2 = H_1 + H_d - (k_0 + 1)r_2 - e_1 - r_2 + \dot{\boldsymbol{q}}_d\tilde{\boldsymbol{\theta}} + \dot{u}_2 \tag{25}$$

where $\dot{u}_2(t)$ is considered as a virtual control input and can be designed as

$$\dot{u}_2 = (k_0 + 1)\, e_3 - 2b\mathrm{sgn}(r_1) \tag{26}$$

Authorized licensed use limited to: Kent State University Libraries. Downloaded on September 20,2023 at 17:54:05 UTC from IEEE Xplore. Restrictions apply.

where k_0 and b are positive control gains. By integrating (26), one has

$$u_2 = \int_0^t \left[(k_0+1)\, e_3 - 2b\mathrm{sgn}(r_1)\right] d\tau \tag{27}$$

which can be proven to be continuous (some brief analysis will be provided in Remark 1). Furthermore, from (14) and (27), the control law (13) can be rearranged as follows:

$$u = \frac{1}{w}\left\{-\boldsymbol{q}_d\hat{\boldsymbol{\theta}} + \int_0^t \left[(k_0+1)\, e_3 - 2b\mathrm{sgn}(r_1)\right] d\tau\right\}. \tag{28}$$

Considering (14) and (27), since $u_1(t)$ and $u_2(t)$ are both continuous, the entire controller $u(t)$ is also continuous. By using the update law (21), the estimation $\hat{\boldsymbol{\theta}}(t)$ can be solved by

$$\hat{\boldsymbol{\theta}} = \boldsymbol{\beta}\dot{\boldsymbol{q}}_d^{\mathrm{T}} r_1\big|_0^t - \boldsymbol{\beta}\int_0^t \left(\ddot{\boldsymbol{q}}_d^{\mathrm{T}} r_1 - \dot{\boldsymbol{q}}_d^{\mathrm{T}}\lambda_2 r_1\right) d\tau + \hat{\boldsymbol{\theta}}(0) \tag{29}$$

where $\hat{\boldsymbol{\theta}}(0)$ is the initial estimate value of $\hat{\boldsymbol{\theta}}(t)$. As shown in (29), the solution of $\hat{\boldsymbol{\theta}}(t)$ does not depend on the signal $r_2(t)$, which is difficult to measure. Then, by inserting (26), it can be obtained from (25) that

$$\begin{aligned}\dot{r}_2 = {} & H_1 + H_d + (k_0+1)\, e_3 - 2b\mathrm{sgn}(r_1) - (k_0+1)r_2 \\ & - e_1 - r_2 + \dot{\boldsymbol{q}}_d\tilde{\boldsymbol{\theta}}.\end{aligned} \tag{30}$$

In the next section, a theorem will be provided to prove the closed-loop stability.

Remark 1: The designed controller in (28) is continuous, which can be proven by providing some discussions on the term $\int_0^t \mathrm{sgn}(r_1(\tau))d\tau$. To this end, by defining $g_c = \int_0^t \mathrm{sgn}(r_1(\tau))\, d\tau$, one can obtain that $|g_c(t_2) - g_c(t_1)| = \left|\int_{t_1}^{t_2}\mathrm{sgn}(r_1(\tau))\, d\tau\right| \le |t_2 - t_1|\ \forall t_1,\, t_2 > 0$, where $|\mathrm{sgn}(r_1)| \le 1\ \forall r_1 \in \mathbb{R}$ is utilized. Furthermore, for any ε, we let $\delta = \varepsilon$. Then, as long as $|t_2 - t_1| < \delta$, we always have that $\left|g_c(t_2) - g_c(t_1)\right| < \varepsilon$, and hence, the term $\int_0^t \mathrm{sgn}(r_1(\tau))d\tau$ can be proven to be continuous by applying the $\varepsilon - \delta$ definition for continuity.

IV. Stability Analysis

First, we present the following lemma.

Lemma 1: The functions $H_1(t), H_d(t)$, and $\dot{H}_d(t)$ are bounded in the sense that

$$\|H_1\|_\infty \le \varphi\|\boldsymbol{\sigma}\|, \quad \|H_d\|_\infty \le \epsilon_1, \|\dot{H}_d\|_\infty \le \epsilon_2 \tag{31}$$

where $\varphi, \epsilon_1,$ and ϵ_2 are positive constants, and the error vector $\boldsymbol{\sigma} \in \mathbb{R}^{5\times 1}$ is given as

$$\boldsymbol{\sigma} \triangleq [r_2, e, e_1, e_2, e_3]^{\mathrm{T}} = [\sigma_1, \ldots, \sigma_5]^{\mathrm{T}}. \tag{32}$$

Proof: First, from (19) and (20), the equations can be calculated as follows:

$$\begin{aligned}\ddot{e} &= r_2 - (\lambda_1+\lambda_2)\, e_1 - e_3 + \lambda_1^2 e \\ \dot{e}_1 &= r_2 - \lambda_2 e_1 - e_3, \quad \dot{e} = e_1 - \lambda_1 e.\end{aligned} \tag{33}$$

By using the mean value theorem, based on (32) and (33), the following equation can be derived:

$$\begin{aligned}&\dot{\xi}_1\left(x, \dot{x}, \ddot{x}, e_2, e_3, r_2, t\right) - \dot{\xi}_{1d}\left(x_d, \dot{x}_d, \ddot{x}_d, 0, 0, 0, t\right) \\ &\quad = f_1(\sigma_1) + f_2(\sigma_2) + f_3(\sigma_3) + f_4(\sigma_4) + f_5(\sigma_5) \\ &\quad = \left.\frac{\partial \dot{f}_1}{\partial \sigma_1}\right|_{\sigma_1 = z_1} \cdot \sigma_1 + \left.\frac{\partial \dot{f}_2}{\partial \sigma_2}\right|_{\sigma_2 = z_2} \cdot \sigma_2 + \left.\frac{\partial \dot{f}_3}{\partial \sigma_3}\right|_{\sigma_3 = z_3} \cdot \sigma_3 \\ &\qquad + \left.\frac{\partial \dot{f}_4}{\partial \sigma_4}\right|_{\sigma_4 = z_4} \cdot \sigma_4 + \left.\frac{\partial \dot{f}_5}{\partial \sigma_5}\right|_{\sigma_5 = z_5} \cdot \sigma_5 \\ &\quad = \boldsymbol{\nu}\cdot\boldsymbol{\sigma}\end{aligned} \tag{34}$$

where $f_i(\sigma_i)'s, i = 1, \ldots, 5$ are functions of $\sigma_i's$, and $\boldsymbol{\nu} \in \mathbb{R}^{1\times 5}$ is defined as follows:

$$\boldsymbol{\nu} \triangleq \left[\left.\frac{\partial \dot{f}_1}{\partial \sigma_1}\right|_{\sigma_1 = z_1}, \ldots, \left.\frac{\partial \dot{f}_5}{\partial \sigma_5}\right|_{\sigma_5 = z_5}\right] \tag{35}$$

in which $z_i's$ are constants chosen within the ranges of $\sigma_i's$, $i = 1, \ldots, 5$. Hence, from (34) and (35), by applying the Cauchy inequality, the upper bound of (34) can be derived as follows:

$$\left|\dot{\xi}_1 - \dot{\xi}_{1d}\right| \le \|\boldsymbol{\nu}\|\|\boldsymbol{\sigma}\|. \tag{36}$$

By inserting (33), (34), and (36) into (24) and making some mathematical arrangements, we have

$$\|H_1\|_\infty = |H_1| \le \|\boldsymbol{\nu}\|\|\boldsymbol{\sigma}\| + \|\boldsymbol{\rho}\|\|\boldsymbol{\sigma}\| \le \varphi\|\boldsymbol{\sigma}\| \tag{37}$$

where

$$\boldsymbol{\rho} = \begin{bmatrix} \left|\lambda_1 + \lambda_2 + 1 - \boldsymbol{q}_d\boldsymbol{\beta}\dot{\boldsymbol{q}}_d^{\mathrm{T}}\right| \\ \left|\lambda_1^3\right| \\ \left|2 - \lambda_1\left(\lambda_1 + \lambda_2\right) - \lambda_2^2\right| \\ 1 \\ \left|\lambda_1 + \lambda_2 + 1\right| \end{bmatrix}^{\mathrm{T}} \tag{38}$$

and φ is a constant satisfying $\varphi \ge \|\boldsymbol{\nu}\| + \|\boldsymbol{\rho}\|$. Obviously, based on (12) and (24), the functions $H_d(t)$ and $\dot{H}_d(t)$ are bounded such that

$$\|H_d\|_\infty \le \epsilon_1, \quad \|\dot{H}_d\|_\infty \le \epsilon_2 \tag{39}$$

where ϵ_1 and ϵ_2 are positive constants. Thus, Lemma 1 is proven. ■

Then, the main stability analysis is proceeded with the following theorem.

Theorem 1: If the following conditions are satisfied:

$$b > \epsilon_1 + \frac{1}{\lambda_2}\epsilon_2, \quad \lambda_1 > \frac{1}{2}, \quad \lambda_2 > \frac{1}{2}, \quad k_0 \ge \frac{\varphi^2}{y} \tag{40}$$

then the tracking error $e(t)$ asymptotically converges to zero by the proposed controller (28), in the sense that

$$\|e(t)\| \to 0 \text{ as } t \to \infty. \tag{41}$$

Authorized licensed use limited to: Kent State University Libraries. Downloaded on September 20,2023 at 17:54:05 UTC from IEEE Xplore. Restrictions apply.

Proof: A scalar function $V(t)$ is chosen as follows (which will be proven to be a Lyapunov function candidate next):

$$\begin{aligned} V &\triangleq \frac{1}{2}r_2^2+\frac{1}{2}e^2+\frac{1}{2}e_1^2+\frac{1}{2}e_2^2+\frac{1}{2}e_3^2 \\ &\quad+(2b|r_1|-H_d r_1)+\frac{1}{2}\tilde{\boldsymbol{\theta}}^{\mathrm{T}}\boldsymbol{\beta}^{-1}\tilde{\boldsymbol{\theta}} \\ &\triangleq \frac{1}{2}\|\boldsymbol{\Lambda}\|^2+\Omega \end{aligned} \tag{42}$$

where $\boldsymbol{\Lambda}\triangleq[e^{\mathrm{T}},e_1^{\mathrm{T}},e_2^{\mathrm{T}},e_3^{\mathrm{T}},r_2^{\mathrm{T}},\tilde{\boldsymbol{\theta}}^{\mathrm{T}}]^{\mathrm{T}}$, $\Omega=2b|r_1|-H_d r_1$. Because $b>\epsilon_1+\frac{1}{\lambda_2}\epsilon_2$, along with (39), one has

$$(2b-\|H_d\|_\infty)\,|r_1|\geq b|r_1|\geq 0. \tag{43}$$

Also, it can be derived that

$$H_d r_1\leq\|H_d\|_\infty|r_1|\Rightarrow -H_d r_1\geq-\|H_d\|_\infty|r_1|. \tag{44}$$

By adding $2b|r_1|$ to both sides of (44), one can obtain

$$2b|r_1|-H_d r_1\geq 2b|r_1|-\|H_d\|_\infty|r_1|. \tag{45}$$

Then, based on (43) and (45), an inequality is obtained as follows:

$$2b|r_1|-H_d r_1\geq b|r_1|\geq 0. \tag{46}$$

Obviously, because $-H_d r_1\leq\|H_d\|_\infty|r_1|$, it is implied that

$$2b|r_1|-H_d r_1\leq(2b+\|H_d\|_\infty)\,|r_1|. \tag{47}$$

From (42) and (47), we may derive that

$$0\leq h_1\|\boldsymbol{\Lambda}\|^2+b|r_1|\leq V\leq h_2\|\boldsymbol{\Lambda}\|^2+(2b+\|H_d\|_\infty)\,|r_1| \tag{48}$$

where $h_1=\min\{\frac{1}{2},\frac{1}{2}\lambda_{\min}\{\boldsymbol{\beta}^{-1}\}\}$, $h_2=\max\{\frac{1}{2},\frac{1}{2}\lambda_{\max}\{\boldsymbol{\beta}^{-1}\}\}$, and $\lambda_{\min}$ and $\lambda_{\max}$ are the minimum and the maximum eigenvalues of $\boldsymbol{\beta}^{-1}$, respectively. Hence, it is implied from (48) that $V(t)$ is nonnegative. In addition, from (42), the equilibrium point is given as follows:

$$\boldsymbol{\Lambda}_{ep}=[e^{\mathrm{T}},e_1^{\mathrm{T}},e_2^{\mathrm{T}},e_3^{\mathrm{T}},r_1^{\mathrm{T}},r_2^{\mathrm{T}},\tilde{\boldsymbol{\theta}}^{\mathrm{T}}]^{\mathrm{T}}=\mathbf{0}. \tag{49}$$

Based on (42) and (49), $V(t)=0$ if and only if $\boldsymbol{\Lambda}_{ep}=\mathbf{0}$. Hence, from the above analysis, $V(t)$ is *positive definite* and thus is a Lyapunov function candidate. Furthermore, to facilitate the subsequent analysis, the following vector $\boldsymbol{N}\in\mathbb{R}^2$ is defined:

$$\boldsymbol{N}\triangleq[\boldsymbol{\Lambda}^{\mathrm{T}},\sqrt{\Omega}]^{\mathrm{T}} \tag{50}$$

and the differential equation of $\boldsymbol{N}(t)$ is defined as $\dot{\boldsymbol{N}}\triangleq R(\boldsymbol{N},t)$, which is continuous except in the set $\{\boldsymbol{N}:r_1=0\}$. Then, let $\boldsymbol{N}(t)$ denote a Filippov continuous solution to $\dot{\boldsymbol{N}}=R(\boldsymbol{N},t)$, such that $\dot{\boldsymbol{N}}\in^{\text{a.e.}}K[R](\boldsymbol{N})$, where $K[\cdot]$ is an upper semicontinuous set-valued map in [35]. Based on the Filippov theory, if we define the time derivative of $V(\boldsymbol{N})$ as $\dot{V}(\boldsymbol{N})$, then $\dot{V}(\boldsymbol{N})$ exists almost everywhere (a.e.), such that $\dot{V}(\boldsymbol{N})\in^{\text{a.e.}}\dot{\tilde{V}}(\boldsymbol{N})$, and $\dot{\tilde{V}}(\boldsymbol{N})$ is given as follows:

$$\begin{aligned} \dot{\tilde{V}} &\triangleq \bigcap_{\delta\in\partial V(\boldsymbol{N})}\delta^{\mathrm{T}}\left(K\left[\dot{\boldsymbol{\Lambda}}^{\mathrm{T}},\dot{\Omega}/2\sqrt{\Omega}\right]^{\mathrm{T}}\right) \\ &\subset[\boldsymbol{\Lambda}^{\mathrm{T}},2\sqrt{\Omega}]\left(K\left[\dot{\boldsymbol{\Lambda}}^{\mathrm{T}},\dot{\Omega}/2\sqrt{\Omega}\right]^{\mathrm{T}}\right) \end{aligned} \tag{51}$$

where $\partial V(\boldsymbol{N})$ represents the generalized gradient of $V(\boldsymbol{N})$, and $\delta\in\partial V(\boldsymbol{N})$ is introduced by the Filippov theory [35]. After taking the derivative of $V(t)$ in (42), it can be obtained on the basis of (51) that

$$\begin{aligned} \dot{\tilde{V}} &\subset r_2K[\dot{r}_2]+e\dot{e}+e_1\dot{e}_1+e_2\dot{e}_2+e_3\dot{e}_3 \\ &\quad+2bK[\mathrm{sgn}(r_1)]\dot{r}_1-\dot{H}_d r_1-H_d\dot{r}_1+\tilde{\boldsymbol{\theta}}^{\mathrm{T}}\boldsymbol{\beta}^{-1}\dot{\tilde{\boldsymbol{\theta}}}. \end{aligned} \tag{52}$$

By inserting (19) and (30) into (52), after making some mathematical arrangements, (52) can be rewritten into the following form:

$$\begin{aligned} \dot{\tilde{V}} &\subset r_2H_d-2br_2K[\mathrm{sgn}(r_1)]-e_1r_2+r_2H_1+r_2e_3\,(k_0+1) \\ &\quad-(k_0+1)\,r_2^2-r_2^2+\left[r_2\dot{\boldsymbol{q}}_d\tilde{\boldsymbol{\theta}}-\tilde{\boldsymbol{\theta}}^{\mathrm{T}}\boldsymbol{\beta}^{-1}\,(\boldsymbol{\beta}\dot{\boldsymbol{q}}_d r_2)\right]+ee_1 \\ &\quad-\lambda_1e^2+e_1\dot{e}_1+e_2e_3-\lambda_2e_2^2-e_3^2-r_2e_3\,(k_0+1) \\ &\quad+e_1e_3-e_2e_3+2bK[\mathrm{sgn}(r_1)]\dot{r}_1-\dot{H}_d r_1-H_d\dot{r}_1. \end{aligned} \tag{53}$$

Then, on the basis of the two expressions of $r_2(t)$ in (20), respectively, the first three terms of (53) become

$$\begin{aligned} r_2H_d-2br_2K[\mathrm{sgn}(r_1)] &= (\dot{r}_1+\lambda_2r_1)\,H_d \\ &\quad-2b\,(\dot{r}_1+\lambda_2r_1)\,K[\mathrm{sgn}(r_1)] \\ e_1r_2 &= e_1\,(\dot{e}_1+\lambda_2e_1+e_3)\,. \end{aligned} \tag{54}$$

By inserting (54), the following conclusion is obtained from (53):

$$\begin{aligned} \dot{\tilde{V}} &\subset -2r_2^2-\lambda_1e^2-\lambda_2e_1^2-\lambda_2e_2^2-e_3^2+ee_1-k_0r_2^2 \\ &\quad-2b\lambda_2K[\mathrm{sgn}(r_1)]r_1+\lambda_2H_dr_1-\dot{H}_dr_1+r_2H_1. \end{aligned} \tag{55}$$

It is worth mentioning that $K[\mathrm{sgn}(r_1)]r_1=\mathrm{SGN}(r_1)r_1=|r_1|$, where the definition of $\mathrm{SGN}(\cdot)$ can be found in [36]. Considering (39), it can be obtained that

$$\begin{aligned} ee_1 &\leq \frac{1}{2}e^2+\frac{1}{2}e_1^2, \lambda_2r_1H_d\leq\lambda_2\|H_d\|_\infty|r_1| \\ \dot{H}_dr_1 &\leq\|\dot{H}_d\|_\infty|r_1|, r_2H_1\leq|r_2||H_1|. \end{aligned} \tag{56}$$

From (55) and (56), one has

$$\begin{aligned} \dot{\tilde{V}} &\overset{\text{a.e.}}{\leq}\left[-2r_2^2-\left(\lambda_1-\frac{1}{2}\right)e^2-\left(\lambda_2-\frac{1}{2}\right)e_1^2-\lambda_2e_2^2-e_3^2\right] \\ &\quad-2\lambda_2b|r_1|+\lambda_2\|H_d\|_\infty|r_1|+\|\dot{H}_d\|_\infty|r_1|+|r_2||H_1|-k_0r_2^2. \end{aligned} \tag{57}$$

Authorized licensed use limited to: Kent State University Libraries. Downloaded on September 20,2023 at 17:54:05 UTC from IEEE Xplore. Restrictions apply.

Also, from (40), the following inequalities can be derived:

$$-\lambda_2 b|r_1| \le -(\lambda_2\epsilon_1+\epsilon_2)\,|r_1|, \|\dot{H}_d\|_\infty|r_1| \le \epsilon_2|r_1|$$
$$\lambda_2\|H_d\|_\infty|r_1| \le \lambda_2\epsilon_1|r_1|, |r_2||H_1| \le \varphi\|\boldsymbol{\sigma}\||r_2|. \quad (58)$$

Hence, by inserting (58), the following inequality can be further obtained from (57):

$$\begin{aligned}\dot{\tilde{V}} &\overset{\text{a.e.}}{\le} \left[-2r_2^2-\left(\lambda_1-\frac{1}{2}\right)e^2-\left(\lambda_2-\frac{1}{2}\right)e_1^2-\lambda_2 e_2^2-e_3^2\right]\\ &\quad+\varphi\|\boldsymbol{\sigma}\||r_2|-k_0r_2^2-\lambda_2 b|r_1|\\ &\overset{\text{a.e.}}{\le} -\min\left\{\lambda_1-\frac{1}{2},\lambda_2-\frac{1}{2},1\right\}\|\boldsymbol{\sigma}\|^2-\lambda_2 b|r_1|\\ &\quad+\varphi\|\boldsymbol{\sigma}\||r_2|-k_0r_2^2\\ &\overset{\text{a.e.}}{\le} -y\|\boldsymbol{\sigma}\|^2+\frac{\varphi^2\|\boldsymbol{\sigma}\|^2}{k_0} \quad (59)\end{aligned}$$

where $y=\min\{\lambda_1-\frac{1}{2},\lambda_2-\frac{1}{2},1\}$. According to (59), it can be obtained that

$$\dot{\tilde{V}} \overset{\text{a.e.}}{\le} -\left(y-\frac{\varphi^2}{k_0}\right)\|\boldsymbol{\sigma}\|^2. \quad (60)$$

Additionally, in (40), if k_0 meets the condition of $k_0 \ge \frac{\varphi^2}{y}$, then one has that $\varphi \le \sqrt{k_0 y}$, $\varphi^2 \le k_0 y$, which leads to $y-\frac{\varphi^2}{k_0} \ge 0$. Therefore, from (60), we have

$$\dot{\tilde{V}} \overset{\text{a.e.}}{\le} 0. \quad (61)$$

Based on (48) and (61), one has

$$V, e, e_1, e_2, r_1, r_2, \tilde{\boldsymbol{\theta}} \in \mathcal{L}_\infty. \quad (62)$$

Considering (62), since $\boldsymbol{\theta}(t)$ contains unknown constants and $\tilde{\boldsymbol{\theta}}(t) \in \mathcal{L}_\infty$, it can be deduced that $\hat{\boldsymbol{\theta}}(t) \in \mathcal{L}_\infty$. From (17), (19), (20), and (62), it can be concluded that $\boldsymbol{q}(t), \boldsymbol{q}_d(t) \in \mathcal{L}_\infty$. Then, (10) and (12) show that $u(t) \in \mathcal{L}_\infty$.

Based on (42) and (61), by using the LaSalle–Yoshizawa theorem [36], the conclusion can be derived that

$$\|\boldsymbol{\sigma}\| \to 0 \text{ as } t \to \infty \Rightarrow \|e(t)\| \to 0 \text{ as } t \to \infty \quad (63)$$

which indicates that Theorem 1 is proven. ■

Remark 2: It is worth mentioning that, from (7) and Theorem 1, if $\Delta u = 0$, then there exists no input saturation problem, and we have $F(u) = u$; even though the calculated value of $u(t)$ exceeds the input constraints, i.e., $\Delta u \neq 0$, the provided stability analysis ensures that the closed-loop system's equilibrium point is asymptotically stable.

V. Experimental Results

A. Self-Built Hardware Platform of PAM Systems

In order to verify the effectiveness of the proposed control method, a few groups of hardware experiments are implemented on a self-built hardware platform as shown in Fig. 3. The platform mainly consists of a Festo DMSP-20-60N-RM-CM-DN fluidic muscle (working air pressure: 0–6 bar, internal diameter: 20 mm, nominal length: 60 mm, and maximum tensile strength: 1500 N), a NOVOtechnik displacement sensor (precision: 0.01 mm), a PCD-dual valve pressure controller (Alicat company), and a real-time measurement and control system, i.e., National Instruments cRIO-9082. The control commands are generated by using LabVIEW, and the control period is 5 ms.

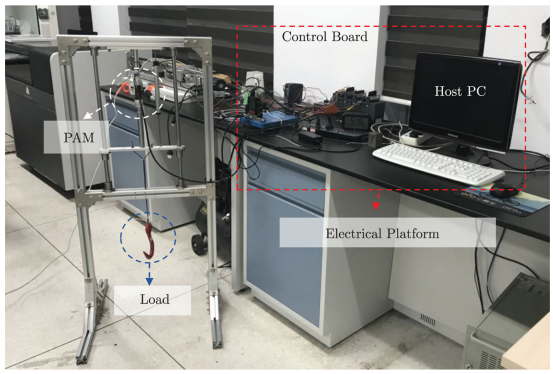

Fig. 3. Self-built experiment platform of PAM systems.

B. Experimental Results and Analysis

For the experiments, the control gains of the proposed controller (28) are first given as follows:

$$m_0 = 0.633\,\text{kg}, \quad g = 9.8\,\text{m/s}^2, \quad w = 222.95$$
$$k_0 = 0.8, \quad b = 220, \quad \lambda_1 = 20, \quad \lambda_2 = 20. \quad (64)$$

Then, in Experiments 1 and 3, the proposed control method is compared with the nonlinear adaptive control method in [27]. The specific expression and the update law of the comparative method are shown as follows:

$$u = -\boldsymbol{q}\hat{\boldsymbol{\theta}} + k_{ap}\dot{e} + k_{ad}e$$
$$\dot{\hat{\boldsymbol{\theta}}} = \boldsymbol{\gamma}\boldsymbol{q}^{\mathrm{T}}(\dot{e}+\lambda e) \quad (65)$$

where $\boldsymbol{\gamma} \in \mathbb{R}^{3\times3}$ is a positive-definite constant diagonal matrix, and k_{ap}, k_{ad}, and λ represent positive control gains, which are carefully tuned as $k_{ap} = 0.4$, $k_{ad} = 0.1$, and $\lambda = 3$. To validate the effectiveness and robustness of the proposed control method, hardware experiments are implemented in the following situations.

Experiment 1 (comparative experiments): In this group, the nonlinear adaptive controller (65) is chosen as the comparative method. The control gains of the proposed method are given in (64). To demonstrate the tracking performance, by tracking different kinds of reference trajectories, the following three cases are considered.

1) *Case 1 (step trajectory):* The amplitude of the step trajectory has a preset value as 7 mm.
2) *Case 2 (sine trajectory):* The amplitude of the sine trajectory is set as 4 mm, the frequency of the waveform is 0.05 Hz, the initial phase is chosen as $-\pi/2$, and the offset of the trajectory is 6 mm.

Authorized licensed use limited to: Kent State University Libraries. Downloaded on September 20,2023 at 17:54:05 UTC from IEEE Xplore. Restrictions apply.

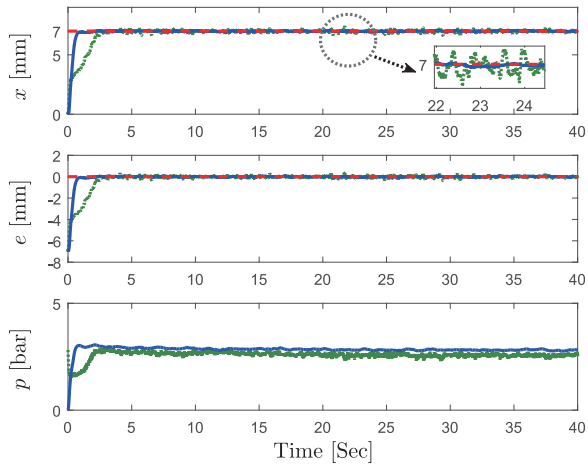

Fig. 4. Results of Experiment 1: Case 1 (*reference trajectories*—red dashed line; *proposed method*—blue solid line; *nonlinear adaptive comparative method*—green dotted line).

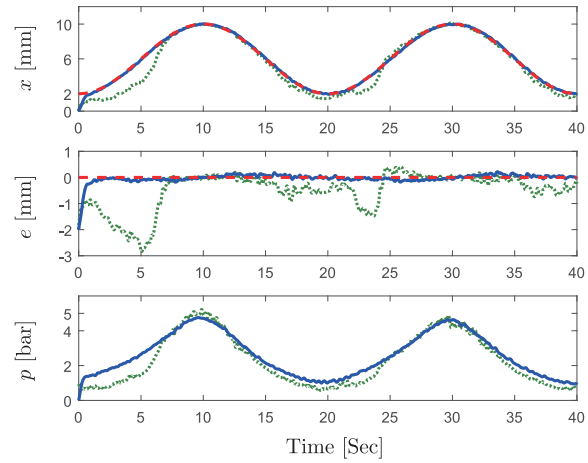

Fig. 5. Results of Experiment 1: Case 2 (*reference trajectories*—red dashed line; *proposed method*—blue solid line; *nonlinear adaptive comparative method*—green dotted line).

3) *Case 3 (triangular-wave trajectory):* The amplitude, the frequency, the initial phase, and the offset of the triangular-wave trajectory are given as 4 mm, 0.05 Hz, $-\pi/2$, and 6 mm, respectively.

The experimental results of Experiment 1 are shown in Figs. 4–6. As shown in Fig. 4, the load displacement $x(t)$ converges to the desired value of 7 mm at about 2 s by applying the proposed method, which is faster than the nonlinear adaptive comparative method (more than 4.7 s). Then, the load displacement $x(t)$ is stabilized at the desired value *without* residual oscillations by the proposed method, while for the comparative method, there still exist residual oscillations. Also, as shown in Figs. 5 and 6, when tracking sine and triangular-wave trajectories, the proposed controller also exhibits rapid and precise tracking performance, with smaller tracking errors than those of the comparative method. Hence, by applying the proposed control method, PAM systems can track various reference trajectories well with satisfactory transient and steady performance.

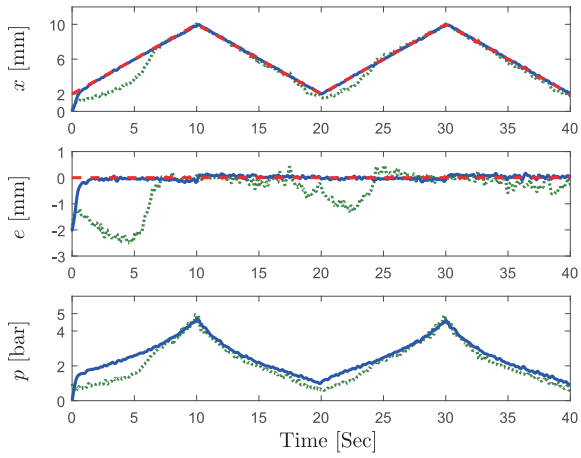

Fig. 6. Results of Experiment 1: Case 3 (*reference trajectories*—red dashed line; *proposed method*—blue solid line; *nonlinear adaptive comparative method*—green dotted line).

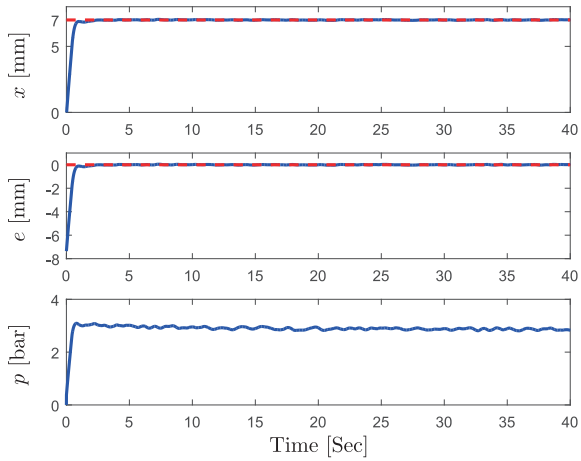

Fig. 7. Results of Experiment 2: Case 1 (*reference trajectories*—red dashed line; *proposed method*—blue solid line).

Experiment 2 (varying load mass): In this group, the load mass is changed to 1.633 kg. The other control gains are the same as those in Experiment 1.

As in Experiment 1, in this group, the three kinds of reference trajectories (i.e., step, sine, and triangular-wave trajectories) are chosen again to verify the tracking performance. The trajectory parameters (e.g., amplitudes, frequencies, etc.) are all the same as those set for Experiment 1.

The experimental results of Experiment 2 are shown in Figs. 7–9. As shown in Figs. 7–9, even when the load mass is changed, the proposed controller can also achieve accurate positioning and satisfactory tracking performance, *without* returning corresponding control gains, by compensating the parametric uncertainties through online estimation. Therefore, the proposed controller can deal with system parametric uncertainties.

Experiment 3 (*external disturbances*): In this group, to further verify the robustness of the proposed control strategy against external disturbances, the load displacement $x(t)$ is disturbed three times during the entire process at about 10, 20, and 30 s,

Authorized licensed use limited to: Kent State University Libraries. Downloaded on September 20,2023 at 17:54:05 UTC from IEEE Xplore. Restrictions apply.

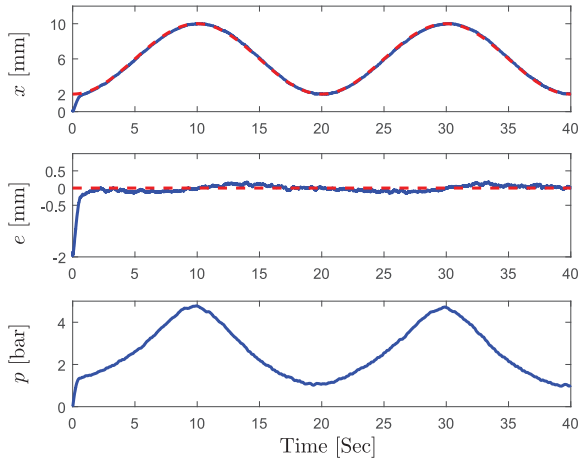

Fig. 8. Results of Experiment 2: Case 2 (*reference trajectories*—red dashed line; *proposed method*—blue solid line).

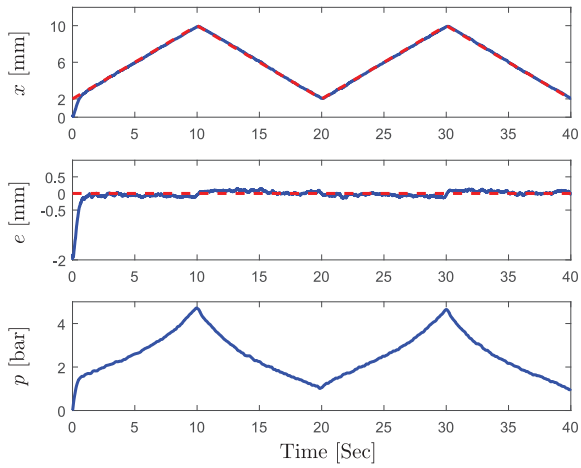

Fig. 9. Results of Experiment 2: Case 3 (*reference trajectories*—red dashed line; *proposed method*—blue solid line).

respectively. The nonlinear adaptive controller (65) is utilized again for comparison.

Fig. 10 shows the experimental results of Experiment 3. It can be seen that the effects induced by these external disturbances are eliminated more effectively and rapidly by the proposed control method than the comparative method. Thus, the proposed control method exhibits satisfactory robustness in the presence of external disturbances.

VI. Conclusion

Aiming at improving the tracking performance and robustness, this paper proposed an adaptive control method for PAM systems *without* linearizing the nonlinear dynamics. Considering unidirectional input constraints, some transforming operations were introduced. To prove the asymptotic convergence of tracking errors, detailed stability analysis was provided with the theoretical analysis. The effectiveness and robustness of the proposed control method were verified by hardware experiments implemented on a self-built experiment platform. In the future, multi-PAM systems (e.g., multilink robots actuated by multi-PAM systems) will be further investigated.

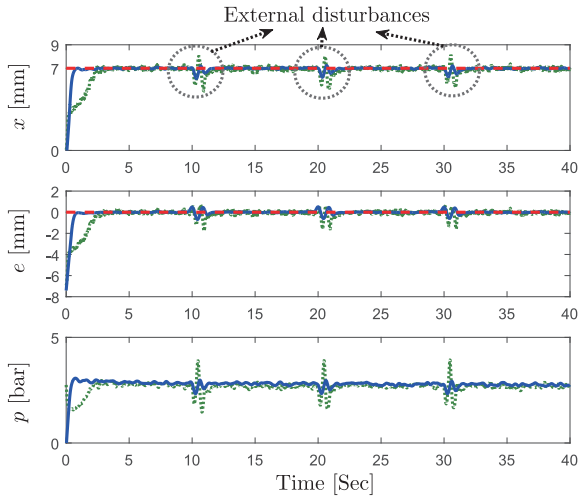

Fig. 10. Results of Experiment 3 (*reference trajectories*—red dashed line; *proposed method*—blue solid line; *nonlinear adaptive comparative method*—green dotted line).

Acknowledgment

The authors would like to express their sincere thanks to the Associate Editor and all the reviewers for the constructive suggestions that have greatly improved the quality of this paper.

References

[1] J. P. Mishra, Q. Xu, X. Yu, and M. Jalili, "Precision position tracking for piezoelectric-driven motion system using continuous third-order sliding mode control," *IEEE/ASME Trans. Mechatronics*, vol. 23, no. 4, pp. 1521–1531, Aug. 2018.

[2] K. Chen, Y. Zhang, J. Yi, and T. Liu, "An integrated physical-learning model of physical human-robot interactions with application to pose estimation in bikebot riding," *Int. J. Robot. Res.*, vol. 35, no. 12, pp. 1459–1476, 2016.

[3] C. Yang, H. Wu, Z. Li, W. He, N. Wang, and C. Y. Su, "Mind control of a robotic arm with visual fusion technology," *IEEE Trans. Ind. Inform.*, vol. 14, no. 9, pp. 3822–3830, Sep. 2018.

[4] W. Sun, Y. Liu, and H. Gao, "Constrained sampled-data ARC for a class of cascaded nonlinear systems with applications to motor-servo systems," *IEEE Trans. Ind. Inform.*, vol. 15, no. 2, pp. 766–776, Feb. 2019.

[5] J. Yang, J. Su, S. Li, and X. Yu, "High-order mismatched disturbance compensation for motion control systems via a continuous dynamic sliding-mode approach," *IEEE Trans. Ind. Inform.*, vol. 10, no. 1, pp. 604–614, Feb. 2014.

[6] Q. Zhou, H. Li, C. Wu, L. Wang, and C. K. Ahn, "Adaptive fuzzy control of nonlinear systems with unmodeled dynamics and input saturation using small-gain approach," *IEEE Trans. Syst., Man, Cybern., Syst.*, vol. 47, no. 8, pp. 1979–1989, Aug. 2017.

[7] R. M. Robinson, C. S. Kothera, and N. M. Wereley, "Variable recruitment testing of pneumatic artificial muscles for robotic manipulators," *IEEE/ASME Trans. Mechatronics*, vol. 20, no. 4, pp. 1642–1652, Aug. 2015.

[8] H. Zheng, M. Wu, and X. Shen, "Pneumatic variable series elastic actuator," *J. Dyn. Syst., Meas., Control*, vol. 138, no. 8, 2016, Art. no. 0810111.

[9] T. Nuchkrua, T. Leephakpreeda, and S. L. Chen, "Experimental validation for fuzzy control of servo pneumatic artificial muscle driven by metal hydride," *Int. J. Fuzzy Syst.*, vol. 18, no. 6, pp. 956–970, 2016.

Authorized licensed use limited to: Kent State University Libraries. Downloaded on September 20,2023 at 17:54:05 UTC from IEEE Xplore. Restrictions apply.

[10] H. Yang, Y. Chen, Y. Sun, and L. Hao, "A novel Kriging-median inverse compensator for modeling and compensating asymmetric hysteresis of pneumatic artificial muscle," *Smart Mater. Struct.*, vol. 27, no. 11, 2018, Art. no. 115019.
[11] S. Terryn, J. Brancart, D. Lefeber, G. V. Assche, and B. Vanderborght, "A pneumatic artificial muscle manufactured out of self-healing polymers that can repair macroscopic damages," *IEEE Robot. Autom. Lett.*, vol. 3, no. 1, pp. 16–21, Jan. 2018.
[12] L. Cveticanin, M. Zukovic, I. Biro, and J. Sarosi, "Mathematical investigation of the stability condition and steady state position of a pneumatic artificial muscle-mass system," *Mech. Mach. Theory*, vol. 125, pp. 196–206, 2018.
[13] B. Tondu, "Modelling of the McKibben artificial muscle: A review," *J. Intell. Mater. Syst. Struct.*, vol. 23, no. 3, pp. 225–253, 2012.
[14] M. R. Sobczyk, V. I. Gervini, E. A. Perondi, and M. A. B. Cunha, "A continuous version of the LuGre friction model applied to the adaptive control of a pneumatic servo system," *J. Franklin Inst.*, vol. 353, no. 13, pp. 3021–3039, 2016.
[15] D. G. Caldwell, G. A. Medrano-Cerda, and M. Goodwin, "Control of pneumatic muscle actuators," *IEEE Control Syst. Mag.*, vol. 15, no. 1, pp. 40–48, Feb. 1995.
[16] C. Ferraresi, W. Franco, and A. M. Bertetto, "Flexible pneumatic actuators: A comparison between the McKibben and the straight fibres muscles," *J. Robot. Mechatronics*, vol. 13, no. 1, pp. 56–63, 2001.
[17] R. W. Colbrunn, G. M. Nelson, and R. D. Quinn, "Modeling of braided pneumatic actuators for robotic control," in *Proc. IEEE/RSJ Int. Conf. Intell. Robots Syst.*, Maui, HI, USA, Oct. 2001, pp. 1964–1970.
[18] D. B. Reynolds, D. W. Repperger, C. A. Phillips, and G. Bandry, "Modeling the dynamic characteristics of pneumatic muscle," *Ann. Biomed. Eng.*, vol. 31, no. 3, pp. 310–317, 2003.
[19] G. Andrikopoulos, G. Nikolakopoulos, I. Arvanitakis, and S. Manesis, "Piecewise affine modeling and constrained optimal control for a pneumatic artificial muscle," *IEEE Trans. Ind. Electron.*, vol. 61, no. 2, pp. 904–916, Feb. 2014.
[20] J. Wu, J. Huang, Y. Wang, and K. Xing, "Nonlinear disturbance observer-based dynamic surface control for trajectory tracking of pneumatic muscle system," *IEEE Trans. Control Syst. Technol.*, vol. 22, no. 2, pp. 440–455, Mar. 2014.
[21] A. Merola, D. Colacino, C. Cosentino, and F. Amato, "Model-based tracking control design, implementation of embedded digital controller and testing of a biomechatronic device for robotic rehabilitation," *Mechatronics*, vol. 52, pp. 70–77, 2018.
[22] Y. Liu, X. Zang, Z. Lin, W. Li, and J. Zhao, "Position control of a bio-inspired semi-active joint with direct inverse hysteresis modeling and compensation," *Adv. Mech. Eng.*, vol. 8, no. 11, pp. 1–8, 2016.
[23] T. V. Minh, T. Tjahjowidodo, H. Ramon, and H. V. Brussel, "Cascade position control of a single pneumatic artificial muscle-mass system with hysteresis compensation," *Mechatronics*, vol. 20, no. 3, pp. 402–414, 2010.
[24] H. I. Chen and M. C. Shih, "Visual control of an automatic manipulation system by microscope and pneumatic actuator," *IEEE Trans. Autom. Sci. Eng.*, vol. 10, no. 1, pp. 215–218, Jan. 2013.
[25] D. Zhang, X. Zhao, and J. Han, "Active model-based control for pneumatic artificial muscle," *IEEE Trans. Ind. Electron.*, vol. 64, no. 2, pp. 1686–1695, Feb. 2017.
[26] D. X. Ba, T. Q. Dinh, and K. K. Ahn, "An integrated intelligent nonlinear control method for a pneumatic artificial muscle," *IEEE/ASME Trans. Mechatronics*, vol. 21, no. 4, pp. 1835–1845, Aug. 2016.
[27] J. H. Lilly, "Adaptive tracking for pneumatic muscle actuators in bicep and tricep configurations," *IEEE Trans. Neural Syst. Rehabil. Eng.*, vol. 11, no. 3, pp. 333–339, Sep. 2003.
[28] R. M. Robinson, C. S. Kothera, R. M. Sanner, and N. M. Wereley, "Nonlinear control of robotic manipulators driven by pneumatic artificial muscles," *IEEE/ASME Trans. Mechatronics*, vol. 20, no. 1, pp. 55–68, Feb. 2016.
[29] N. N. Son, C. V. Kien, and H. P. H. Anh, "A novel adaptive feed-forward-PID controller of a SCARA parallel robot using pneumatic artificial muscle actuator based on neural network and modified differential evolution algorithm," *Robot. Auton. Syst.*, vol. 96, pp. 65–80, 2017.
[30] A. P. Aguiar and J. P. Hespanha, "Trajectory-tracking and path-following of underactuated autonomous vehicles with parametric modeling uncertainty," *IEEE Trans. Autom. Control*, vol. 52, no. 8, pp. 1362–1379, Aug. 2007.
[31] H. Sira-Ramírez, J. Linares-Flores, C. García-Rodríguez, and M. A. Contreras-Ordaz, "On the control of the permanent magnet synchronous motor: An active disturbance rejection control approach," *IEEE Trans. Control Syst. Technol.*, vol. 22, no. 5, pp. 2056–2063, Sep. 2014.
[32] J. Wang, S. He, and D. Lin, "Robust backstepping control for a class of nonlinear systems using generalized disturbance observer," *Int. J. Control, Autom. Syst.*, vol. 14, no. 6, pp. 1475–1483, 2016.
[33] B. Xian, D. M. Dawson, M. S. de Queiroz, and J. Chen, "A continuous asymptotic tracking control strategy for uncertain nonlinear systems," *IEEE Trans. Autom. Control*, vol. 49, no. 7, pp. 1206–1211, Jul. 2004.
[34] N. Fischer, D. Hughes, P. Walters, E. M. Schwartz, and W. E. Dixon, "Nonlinear RISE-based control of an autonomous underwater vehicle," *IEEE Trans. Robot.*, vol. 30, no. 4, pp. 845–852, Aug. 2014.
[35] B. Paden and S. Sastry, "A calculus for computing Filippov's differential inclusion with application to the variable structure control of robot manipulators," *IEEE Trans. Circuits Syst.*, vol. CAS-34, no. 1, pp. 73–82, Jan. 1987.
[36] N. Fischer, R. Kamalapurkar, and W. E. Dixon, "LaSalle-Yoshizawa corollaries for nonsmooth systems," *IEEE Trans. Autom. Control*, vol. 58, no. 9, pp. 2333–2338, Sep. 2013.

Ning Sun (S'12–M'14) received the B.S. degree in measurement and control technology and instruments from Wuhan University, Wuhan, China, in 2009, and the Ph.D. degree in control theory and control engineering from Nankai University, Tianjin, China, in 2014.

He is currently an Associate Professor with the Institute of Robotics and Automatic Information Systems, College of Artificial Intelligence, Nankai University, Tianjin, China. He is also a Japan Society for the Promotion of Science International Research Fellow with the Faculty of Computer Science and Systems Engineering, Okayama Prefectural University, Okayama, Japan, from Nov. 2018 to Oct. 2019. His research interests include underactuated systems (e.g., cranes) and nonlinear control with applications to mechatronic systems.

Dr. Sun received the First Class Prize of the Wu Wen Jun Artificial Intelligence Natural Science Award, the First Class Prize of the Tianjin Natural Science Award, the Golden Patent Award of Tianjin, the *International Journal of Control, Automation, and Systems* Academic Activity Award, the Outstanding Ph.D. Dissertation Award from the Chinese Association of Automation, etc. He is the Executive Editor for *Measurement and Control* and an Associate Editor (Editorial Board Member) for several journals, including the IEEE ACCESS, the *International Journal of Control, Automation, and Systems*, and the *International Journal of Precision Engineering and Manufacturing*, etc.

Dingkun Liang received the B.S. degree in intelligent science and technology in 2016 from Nankai University, Tianjin, China, where she is currently working toward the Ph.D. degree in control science and engineering, under the supervision of Dr. Ning Sun, with the Institute of Robotics and Automatic Information Systems.

Her research interests include the modeling and control of pneumatic artificial muscle systems and wheeled inverted pendulum robots.

Yiming Wu received the B.S. degree in intelligent science and technology in 2016 from Nankai University, Tianjin, China, where she is currently working toward the Ph.D. degree in control science and engineering, under the supervision of Dr. Ning Sun, with the Institute of Robotics and Automatic Information Systems.

Her research interests include the control of underactuated systems.

Authorized licensed use limited to: Kent State University Libraries. Downloaded on September 20,2023 at 17:54:05 UTC from IEEE Xplore. Restrictions apply.

Yiheng Chen received the B.S. degree in intelligent science and technology in 2018 from Nankai University, Tianjin, China, where she is currently working toward the M.S. degree in control science and engineering, under the supervision of Dr. Ning Sun, with the Institute of Robotics and Automatic Information Systems.

Her research interests include the modeling and nonlinear control of pneumatic artificial muscle systems.

Yanding Qin received the B.Eng. and M.Sc. degrees in industrial design and the Ph.D. degree in mechanical engineering from Tianjin University, Tianjin, China, in 2005, 2007, and 2012, respectively.

From 2009 to 2010, he was a Visiting Scholar with the School of Mechanical Engineering, Purdue University, West Lafayette, IN, USA. From 2012 to 2013, he was a Postdoctoral Research Officer with the Robotics and Mechatronics Research Laboratory, Department of Mechanical and Aerospace Engineering, Monash University, Clayton, Australia. He is currently an Associate Professor with the Institute of Robotics and Automatic Information Systems, College of Artificial Intelligence, Nankai University, Tianjin, China. His research interests include flexure-based mechanism, micro/nanomanipulation, hysteresis modeling and compensation, laser-based measurement, mechanical dynamics, three-dimensional bioprinting, and super-resolution microscopy.

Yongchun Fang (S'00–M'02–SM'08) received the B.S. and M.S. degrees in control theory and applications from Zhejiang University, Hangzhou, China, in 1996 and 1999, respectively, and the Ph.D. degree in electrical engineering from Clemson University, Clemson, SC, USA, in 2002.

From 2002 to 2003, he was a Postdoctoral Fellow with the Sibley School of Mechanical and Aerospace Engineering, Cornell University, Ithaca, NY, USA. He is currently a Professor with the Institute of Robotics and Automatic Information Systems, College of Artificial Intelligence Nankai University, Tianjin, China. His research interests include nonlinear control, visual servoing, control of underactuated systems, and AFM-based nanosystems.

Authorized licensed use limited to: Kent State University Libraries. Downloaded on September 20,2023 at 17:54:05 UTC from IEEE Xplore. Restrictions apply.